# Supplemental Information for:

# Axial Mixing and Vortex Stability to *in-situ* Radial Injection in Taylor-Couette Laminar and Turbulent Flows

*Nikolas Wilkinson*[1] *and Cari Dutcher*[2,*]

[1]Department of Chemical Engineering and Materials Science, University of Minnesota - Twin Cities, 421 Washington Avenue SE, Minneapolis, MN 55455, USA.

[2] Department of Mechanical Engineering, University of Minnesota - Twin Cities, 111 Church Street SE, Minneapolis, MN 55455, USA.

*Corresponding Author Email cdutcher@umn.edu

**Supplemental Image to Concentration Calibration Information**

The concentration of Kalliroscope is measured by quantifying the intensity of light locally reflected by the Kalliroscope solids in solution. Therefore, a calibration of pixel intensity mapped to Kalliroscope concentration was constructed. The pixel intensity of each vortex area is averaged together, producing a single concentration per vortex. Vortex bounds were identified manually by extracting pixel row locations from the video where two vortices meet. For the wavy vortex states, the midpoint of the axial location of the vortex boundary was used. Each vortex is calibrated separately to eliminate variations in brightness in the light sheet and reflectivity differences along the inner cylinder and from the injection port covers. First, the 20 second time frame immediately prior to injection is used to set the zero-concentration light intensity value. The zero-concentration value is used to correct for any reflections in the system and background scattering. Second, the last 20 seconds after complete mixing is averaged together to get the final concentration intensity value, which, again, eliminates any variation in intensity within the light sheet, reflectivity differences along the cylinder, and injection port covers. To reduce high frequency noise from variations in azimuthal reflectivity of the inner cylinder, a 50 frame (1 second) moving average was applied to each time series, using the *movmean* command in MATLAB. The smoothing did not change the mass transfer regression, but improved clarity of the data. The intensity is then linearly scaled to concentration per vortex using the following equation:

$$C = \frac{I - I_o}{I_f - I_o} \times \frac{m}{V_o + {}^{m}/_{\rho}} \qquad \textit{Equation 2}$$

Where C is the concentration of Kalliroscope solution [g/L], I is the instantaneous average pixel intensity, $I_o$ is the zero-concentration intensity, $I_f$ is the final concentration intensity, m is the mass of Kalliroscope injected, and $\rho$ is the density of the Kalliroscope solution, which was measured to be 994.6 ± 1.1 [kg/m$^3$]. $V_o$ is the initial volume of distilled water in the annulus, equal to 1.8 L.

Because the scattering from individual Kalliroscope particles can interact with other Kalliroscope particles in solution, the intensity to concentration profile is not necessarily linear with concentration. To account for this non-linearity an injection of 20 g Kalliroscope in the TTV structure (Re = 6510) was repeated a total of 5 times with 3 min of time in between to allow for the concentrations in each vortex to equilibrate. The concentration profile over time is shown in Figure 2A. The entire concentration profile was then constructed using the linear scaling described above, except that the time after the third injection was used as $I_F$. This modification was made so that the $I_F$ used for calibration is close to the value used for the actual mass transfer experiments. The linearly scaled concentration was then regressed to the expected concentration, shown in Figure 2B. This resulted in the following best fit quadratic scaling:

$$C_{scaled} = -0.003613\, C^2 + 1.108\, C \qquad \textit{Equation 3}$$

Where C is the linearly scaled concentration of Kalliroscope from above and $C_{scaled}$ is the properly scale Kalliroscope concentration [g/L]. The results of this scaling are shown in Figure 2B and primarily only effects Kalliroscope concentrations above 35 g/L, where it reduces the concentration value. The calibration at high loadings is important in the lower Re vortex structures, such as the TWV, where the concentration of Kalliroscope in the vortices near the injection ports can be high. Without this reduction from the non-linear correction, the mass transfer between vortices would appear lower than it is.

**Supplemental Motor Speed Ramp Information**

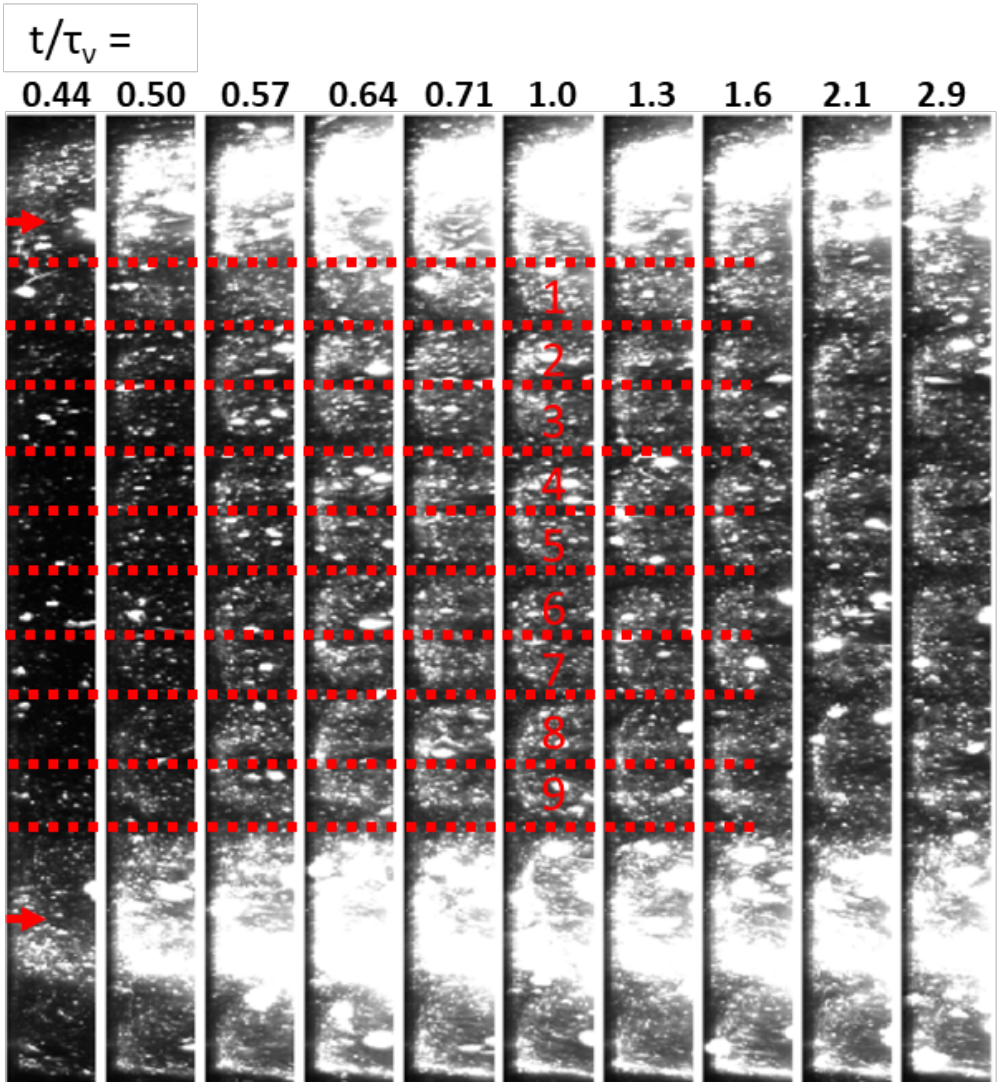


**Supplementary Figure S1:** Mass transfer results for the TTV structure (Re = 10090, $v_{cylinder}$ = 120 cm/s, $\Omega_{cylinder}$ = 2.8 Hz) for a 20 psi (3.1 g/s, 0.32 m/s) 50 g injection (2.7% annulus, $t_{inject}$ = 16 s). Snapshots (0.75 cm wide) of the annulus between injection port rows 3 and 4 after injection illustrating the spatial concentration evolution. The numbers at the top of panel represent the dimensionless time, $t/\tau_v$ ($\tau_v = d^2/\nu$), of each panel. The red arrows indicate the axial location of the injection port row 3 and 4, which are 10 cm apart. The rad, dashed lines indicated the boundaries between vortices. The red numbers indicate the labelling of each vortex.

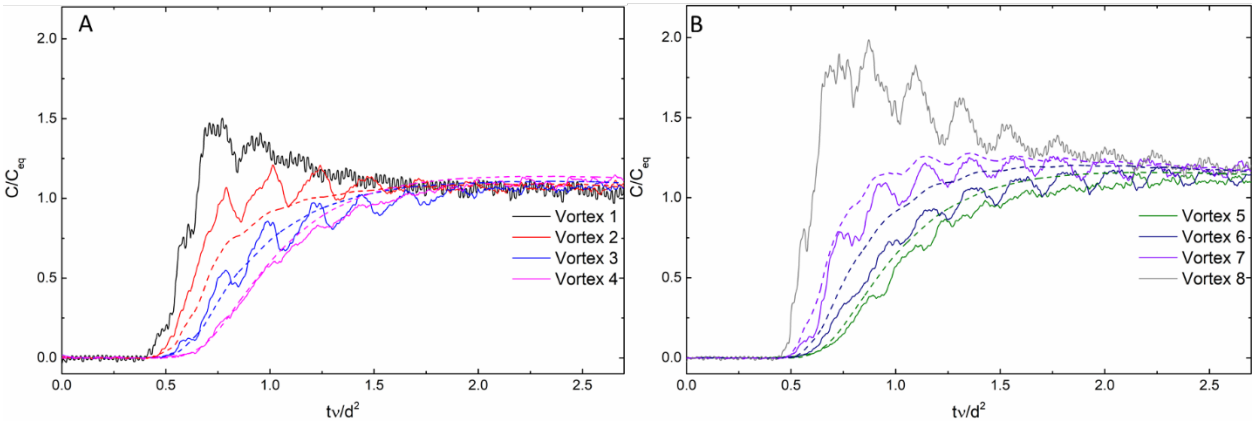


**Supplementary Figure S2:** Mass transfer results for the LWV structure (Re = 615, $v_{cylinder}$ = 7.5 cm/s, $\Omega_{cylinder}$ = 0.17 Hz) for a 20 psi (3.1 g/s, 0.32 m/s) 50 g injection (2.7% annulus, $t_{inject}$ = 16 s). Temporal profile of the concentration in several vortices (solid lines) and the model (dashed lines) using the best fit intermixing coefficient. The y-axis is normalized by the equilibrium concentration of Kalliroscope, 25 g/L, and the x-axis is dimensionless time, time divided by momentum timescale ($\tau_v$ = 70.139 s). The black (Vortex 1) and grey (Vortex 8) lines correspond to the outermost vortices that are used as the input boundary conditions in the model regression. The model is regressed over the entire time profile (extending to $t/\tau_v$ = 8.6 (600 s)), but only the shorter time response is shown here to better show the differences between vortex structures.

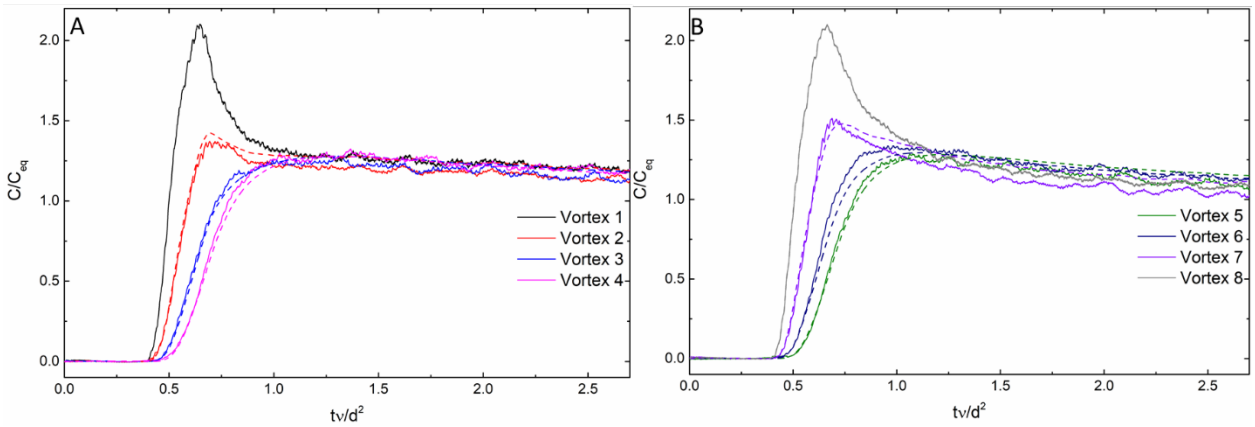


**Supplementary Figure S3:** Injection Mass transfer results for the TWV structure (Re = 2083, $v_{cylinder}$ = 25 cm/s, $\Omega_{cylinder}$ = 0.59 Hz) for a 20 psi (3.1 g/s, 0.32 m/s) 50 g injection (2.7% annulus, $t_{inject}$ = 16 s). Temporal profile of the concentration in several vortices (solid lines) and the model (dashed lines) using the best fit intermixing coefficient. The y-axis is normalized by the equilibrium concentration of Kalliroscope, 25 g/L, and the x-axis is dimensionless time, time divided by momentum timescale ($\tau_v$ = 70.139 s). The black (Vortex 1) and grey (Vortex 8) lines correspond to the outermost vortices that are used as the input boundary conditions in the model regression. The model is regressed over the entire time profile (extending to $t/\tau_v$ = 8.6 (600 s)), but only the shorter time response is shown here to better show the differences between vortex structures.

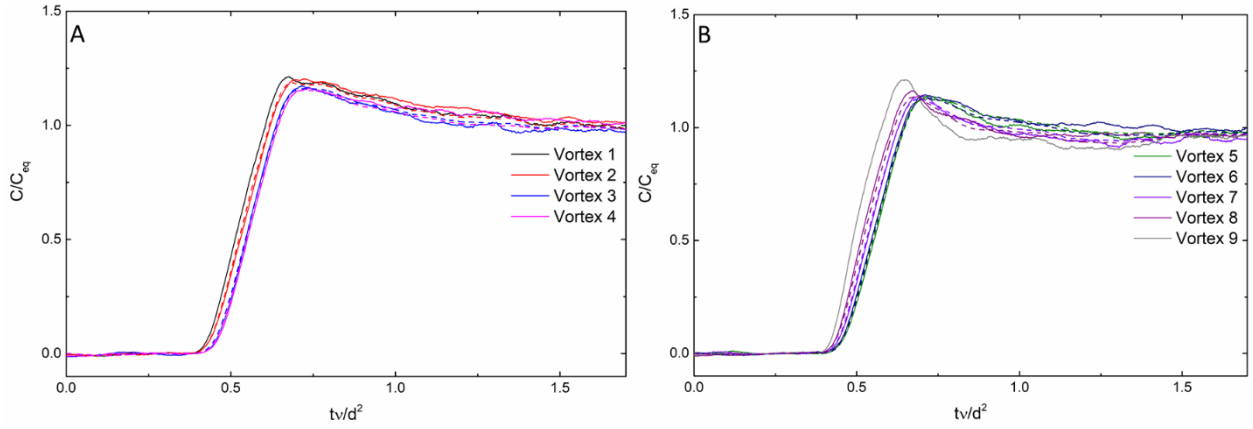


**Supplementary Figure S4:** Mass transfer results for the TTV structure (Re = 10090, $v_{cylinder}$ = 120 cm/s, $\Omega_{cylinder}$ = 2.8 Hz) for a 20 psi (3.1 g/s, 0.32 m/s) 50 g injection (2.7% annulus, $t_{inject}$ = 16 s). Temporal profile of the concentration in several vortices (solid lines) and the model (dashed lines) using the best fit intermixing coefficient. The y-axis is normalized by the equilibrium concentration of Kalliroscope, 25 g/L, and the x-axis is dimensionless time, time divided by momentum timescale ($\tau_v$ = 70.139 s). The black (Vortex 1) and grey (Vortex 9) lines correspond to the outermost vortices that are used as the input boundary conditions in the model regression. The model is regressed over the entire time profile (extending to $t/\tau_v$ = 8.6 (600 s)), but only the shorter time response is shown here to better show the differences between vortex structures.

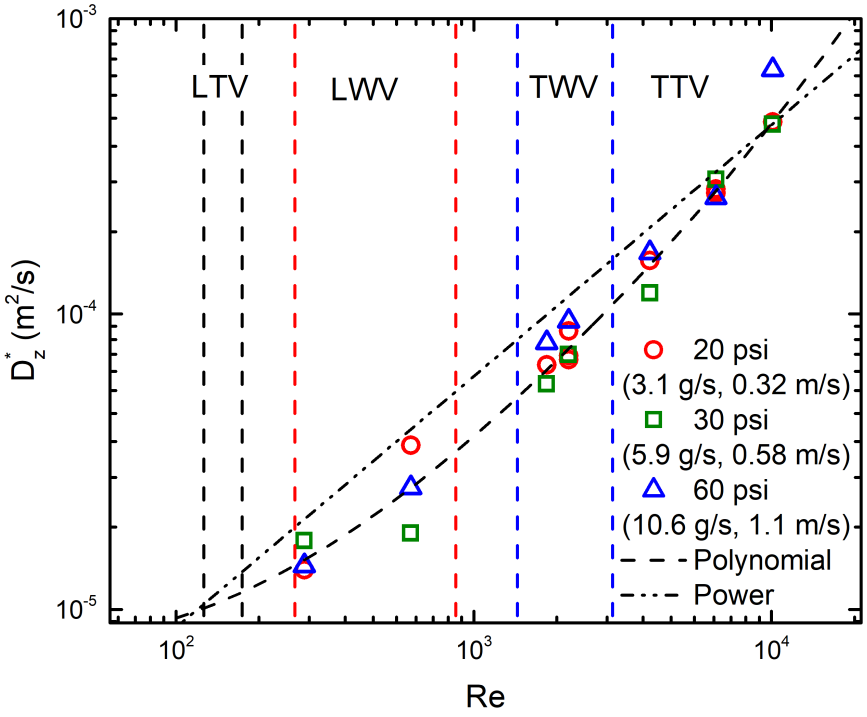


**Supplementary Figure S5:** Imaginary mass transfer coefficient for all injection pressures and vortex flow states explored. The effective dispersion coefficient trend is similar to the intermixing coefficient because the axial wavelengths for all vortices were ~1 cm. All values are from 50 g (2.7% annulus, 4.7 s < $t_{inject}$ < 16 s) injections. The dashed line corresponds to the quadratic best fit, with and $R^2$ of 0.92. The dash dot dot line corresponds to a power law fit, with a $R^2$ of 0.87.

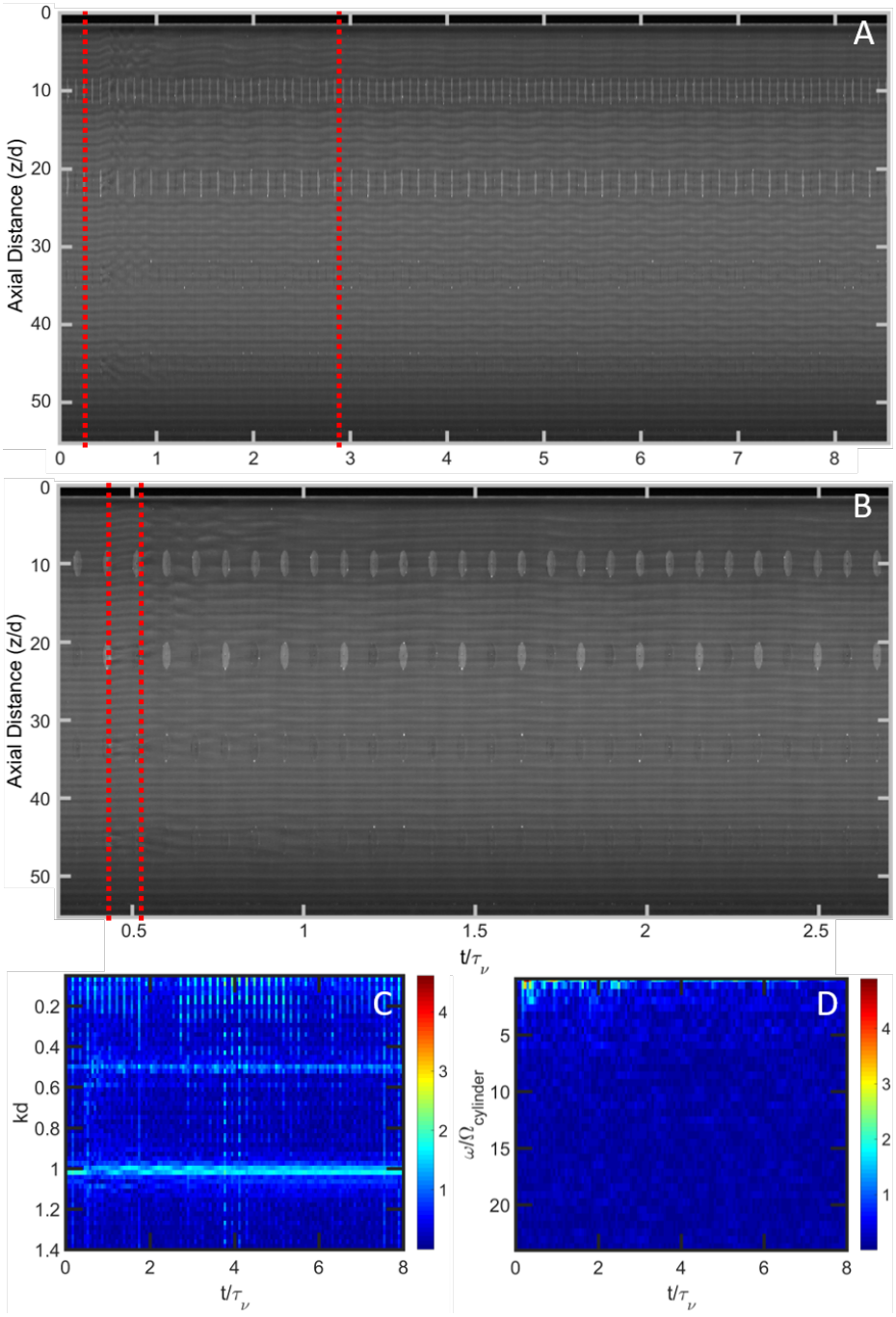


**Supplementary Figure S6:** Space-Time and corresponding Fourier transform plots for LTV (Re = 146, $v_{cylinder}$ = 0.28 cm/s, $\Omega_{cylinder}$ = 0.041 Hz) 20 psi (3.1 g/s, 0.32 m/s) 20 g (1.1% annulus, $t_{inject}$ = 6.4 s), showing stable behavior. The depicted view is of entire annulus height. The axial locations of the injection port rows are z/d = 10, 21, 33, and 45 (8, 18, 28, and 38 cm). The periodic grey spots in are the injection port covers. In the top row, all ports are visible, and in the second row, every other port is visible. A) Space-Time plot showing the entire time response of the vortex structure. The vertical, red dashed lines show the time range that panel B shows. B) Space-Time plot showing the short time response of the vortex during and after injection. The vertical, red dashed lines enclose the injection duration. C) Spatial Fourier transform contour for the entire time domain. D) Temporal Fourier transform contour for the entire time domain. The color represents the log of the magnitude of the complex modulus of the FFT.

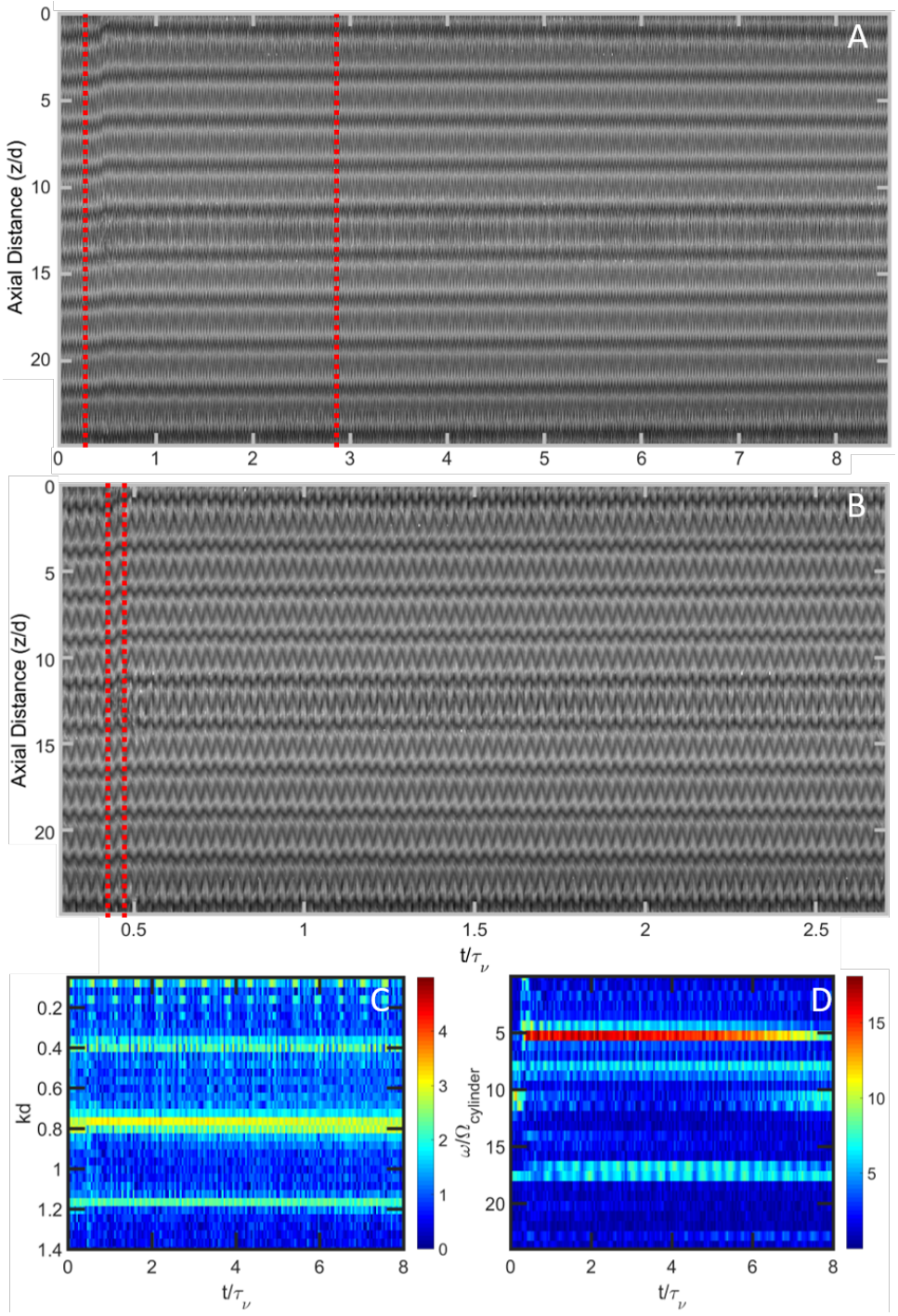


**Supplementary Figure S7:** Space-Time and corresponding Fourier transform plots for LWV (Re = 615, $v_{cylinder}$ = 1.2 cm/s, $\Omega_{cylinder}$ = 0.17 Hz) 30 psi (5.9 g/s, 0.58 m/s) 20 g (1.1% annulus, $t_{inject}$ = 3.4 s), showing stable behavior. The depicted view is between injection port rows 2-4. The axial locations of the injection port rows are z/d = 1.2, 13, and 25 (1, 11 and 21 cm). A) Space-Time plot showing the entire time response of the vortex structure. The vertical, red dashed lines show the time range that panel B shows. B) Space-Time plot showing the short time response of the vortex during and after injection. The vertical, red dashed lines enclose the injection duration. C) Spatial Fourier transform contour for the entire time domain. D) Temporal Fourier transform contour for the entire time domain. The color represents the log of the magnitude of the complex modulus of the FFT.

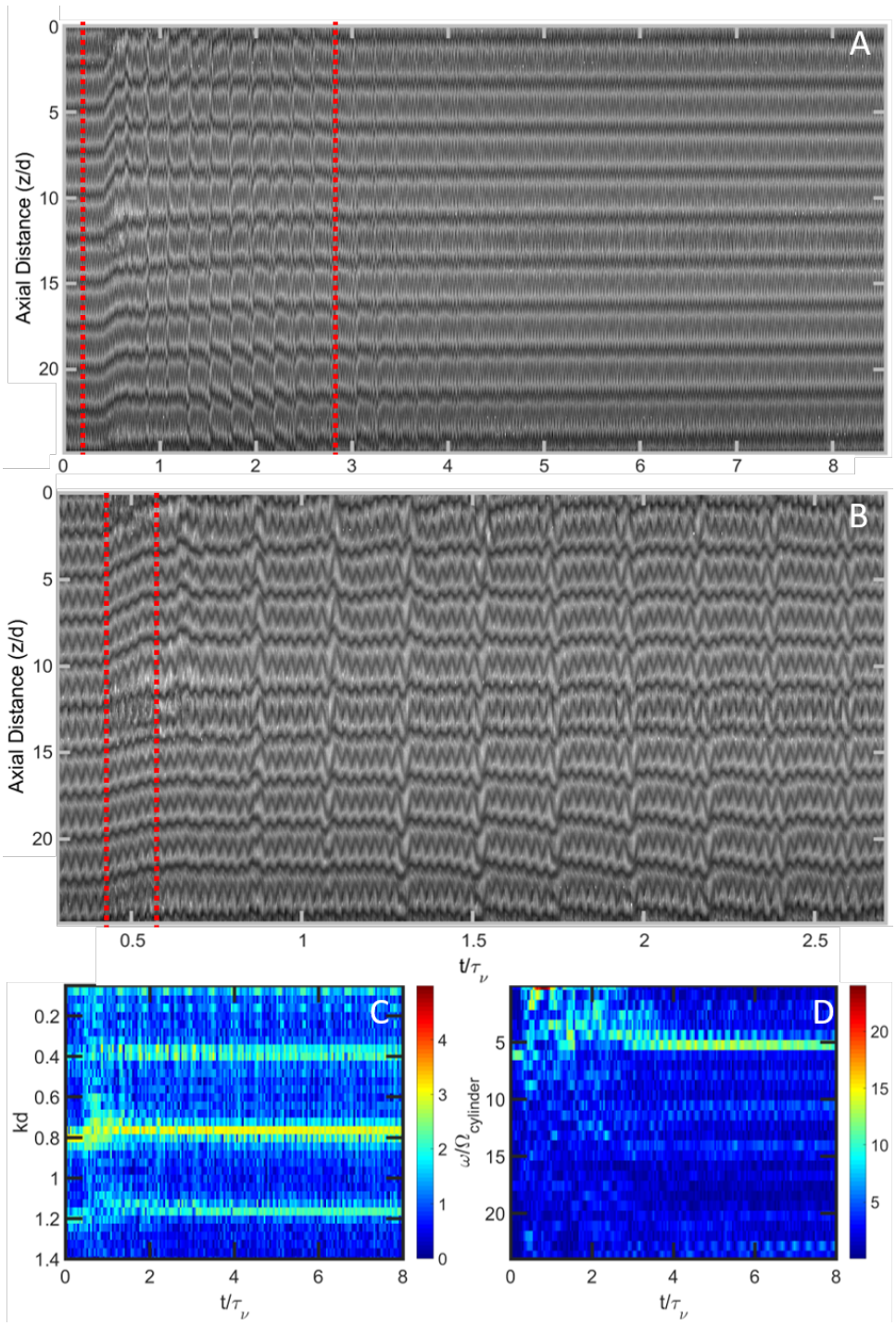


**Supplementary Figure S8:** Space-Time and corresponding Fourier transform plots for LWV (Re = 615, $v_{cylinder}$ = 1.2 cm/s, $\Omega_{cylinder}$ = 0.17 Hz) 60 psi (10.6 g/s, 1.1 m/s) 100 g (5.5% annulus, $t_{inject}$ = 9.5 s), showing unstable behavior. The depicted view is between injection port rows 2-4. The axial locations of the injection port rows are z/d = 1.2, 13, and 25 (1, 11 and 21 cm). A) Space-Time plot showing the entire time response of the vortex structure. The vertical, red dashed lines show the time range that panel B shows. B) Space-Time plot showing the short time response of the vortex during and after injection. The vertical, red dashed lines enclose the injection duration. C) Spatial Fourier transform contour for the entire time domain. D) Temporal Fourier transform contour for the entire time domain. The color represents the log of the magnitude of the complex modulus of the FFT.

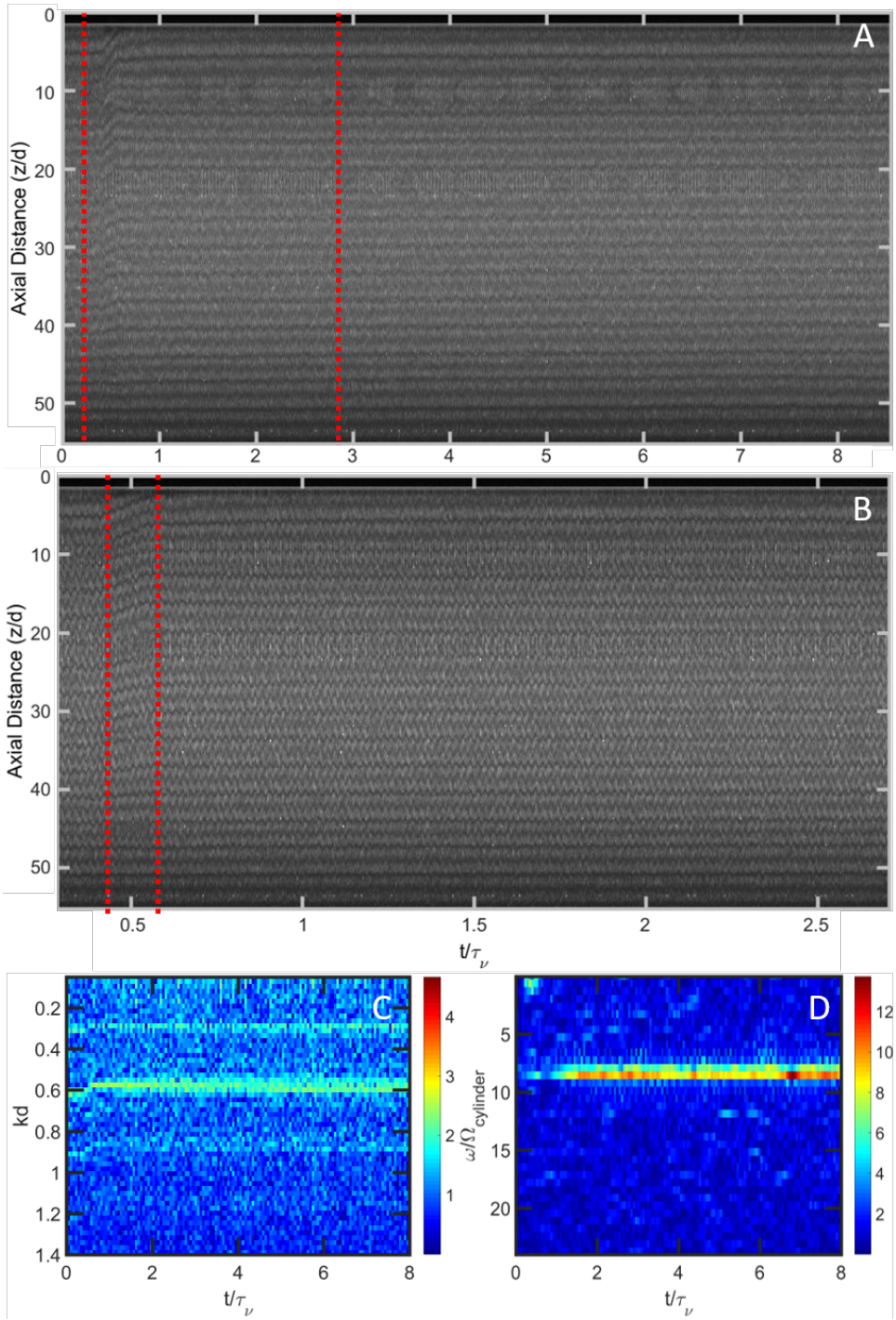


**Supplementary Figure S9:** Space-Time and corresponding Fourier transform plots for TWV (Re = 2083, $v_{cylinder}$ = 4.0 cm/s, $\Omega_{cylinder}$ = 0.59 Hz) 60 psi (10.6 g/s, 1.1 m/s) 100 g (5.5% annulus, $t_{inject}$ = 9.5 s), showing stable behavior. The depicted view is the entire annulus height. The axial locations of the injection port rows are z/d = 10, 21, 33, and 45 (8, 18, 28 and 38 cm). A) Space-Time plot showing the entire time response of the vortex structure. The vertical, red dashed lines show the time range that panel B shows. B) Space-Time plot showing the short time response of the vortex during and after injection. The vertical, red dashed lines enclose the injection duration. C) Spatial Fourier transform contour for the entire time domain. D) Temporal Fourier transform contour for the entire time domain. The color represents the log of the magnitude of the complex modulus of the FFT.

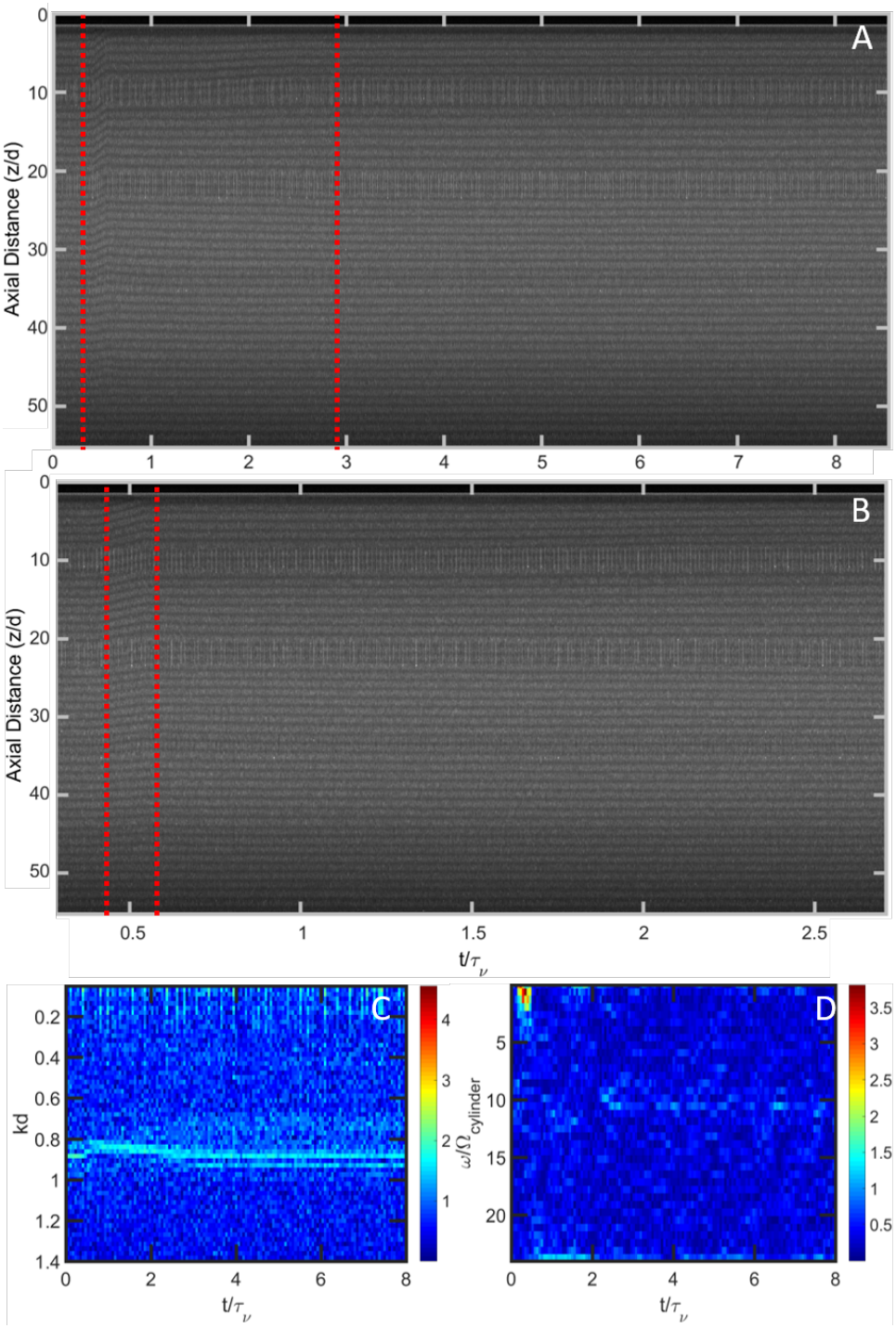


**Supplementary Figure S10:** Space-Time and corresponding Fourier transform plots for TWV (Re = 6510, $v_{cylinder}$ = 19 cm/s, $\Omega_{cylinder}$ = 2.8 Hz) 60 psi (10.6 g/s, 1.1 m/s) 100 g (5.5% annulus, $t_{inject}$ = 9.5 s), showing stable behavior. The depicted view is the entire annulus height. The axial locations of the injection port rows are z/d = 10, 21, 33, and 45 (8, 18, 28 and 38 cm). A) Space-Time plot showing the entire time response of the vortex structure. The vertical, red dashed lines show the time range that panel B shows. B) Space-Time plot showing the short time response of the vortex during and after injection. The vertical, red dashed lines enclose the injection duration. C) Spatial Fourier transform contour for the entire time domain. D) Temporal Fourier transform contour for the entire time domain. The color represents the log of the magnitude of the complex modulus of the FFT.